ANNALS OF
BOTANY
Founded 1887

PART OF A SPECIAL ISSUE ON FUNCTIONAL-STRUCTURAL PLANT GROWTH MODELLING

A functional–structural plant model that simulates whole- canopy gas exchange of grapevine plants (*Vitis vinifera* L.) under different training systems

Jorge A. Prieto[1],*, Gaetan Louarn[2], Jorge Perez Peña[1], Hernán Ojeda[3], Thierry Simonneau[4] and Eric Lebon[4],†

[1]INTA EEA Mendoza, San Martín 3853, Luján de Cuyo (5507), Mendoza, Argentina, [2]INRA, UR4 P3F, Route de Saintes, BP 6, F-86600 Lusignan, France, [3]INRA, UE of Pech Rouge, Gruissan, France and [4]INRA Montpellier SupAgro, UMR759 LEPSE, 2 place Viala, 34060 Montpellier Cedex 01, France
*For correspondence. E-mail prieto.jorge@inta.gob.ar
†Deceased

• **Background and Aims** Scaling from single-leaf to whole-canopy photosynthesis faces several complexities related to variations in light interception and leaf properties. To evaluate the impact of canopy strucuture on gas exchange, we developed a functional–structural plant model to upscale leaf processes to the whole canopy based on leaf N content. The model integrates different models that calculate intercepted radiation, leaf traits and gas exchange for each leaf in the canopy. Our main objectives were (1) to introduce the gas exchange model developed at the plant level by integrating the leaf-level responses related to canopy structure, (2) to test the model against an independent canopy gas exchange dataset recorded on different plant architectures, and (3) to quantify the impact of intra-canopy N distribution on crop photosynthesis.
• **Methods** The model combined a 3D reconstruction of grapevine (*Vitis vinifera*) canopy architecture, a light interception model, and a coupled photosynthesis and stomatal conductance model that considers light-driven variations in N distribution. A portable chamber device was constructed to measure whole-plant gas exchange to validate the model outputs with data collected on different training systems. Finally, a sensitivity analysis was performed to evaluate the impact on C assimilation of different N content distributions within the canopy.
• **Key Results** By considering a non-uniform leaf N distribution within the canopy, our model accurately reproduced the daily pattern of gas exchange of different canopy architectures. The gain in photosynthesis permitted by the non-uniform compared with a theoretical uniform N distribution was about 18 %, thereby contributing to the maximization of C assimilation. By contrast, considering a maximal N content for all leaves in the canopy overestimated net CO_2 exchange by 28 % when compared with the non-uniform distribution.
• **Conclusions** The model reproduced the gas exchange of plants under different training systems with a low error (10 %). It appears to be a reliable tool to evaluate the impact of a grapevine training system on water use efficiency at the plant level.

Key words: *Vitis vinifera*, functional–structural plant model, photosynthesis, transpiration, training system, leaf N content, canopy structure, gas exchange.

INTRODUCTION

Grapevine (*Vitis vinifera*) canopy structure is an important factor determining yield and grape quality (Smart *et al.*, 1990). There is a huge diversity of training systems used worldwide, which results in different canopy architectures adapted to different environments (Carbonneau and Cargnello, 2003; Reynolds and Vanden Heuvel, 2009). Further modifications of canopy structure are also produced during the growing season by viticultural practices such as leaf removal, shoot positioning and green pruning (Smart, 1985). These complex arrangements in canopy architecture produce high spatial and temporal variability in leaf light interception (Louarn *et al.*, 2008*a*), leaf properties (Schultz, 1995) and gas exchange of each individual leaf (Escalona *et al.*, 2003). As a result, water use and photosynthesis may vary considerably with canopy structure. Analysing these variations requires scaling up from the single leaf to the whole canopy to take into account these heterogeneities in

microclimate and individual leaf properties (Niinemets and Tenhunen, 1997). Since existing literature on different grapevine training systems mostly neglects these heterogeneities by considering mean leaves, it is still not clear how canopy structure affects C gain and water use efficiency at the whole-plant level (Medrano *et al.*, 2015).

Functional–structural plant models provide the tools and the framework to accurately describe the canopy structure (i.e. the exact position of plant organs in space), and characterize the distribution of micrometeorological conditions at organ scale, such as intercepted light (Vos *et al.*, 2010). These kinds of model require a detailed 3D description of the plant architecture, which is often tedious and time-consuming, but necessary in order to decipher the interactions between plant structure and physiology (Vos *et al.*, 2010; Sarlikioti *et al.*, 2011). In grapevine, 3D canopy structures have been recorded by digitizing (Mabrouk *et al.*, 1997; Sinoquet *et al.*, 1998), while

the variability of canopy structure has alternatively been captured by statistical modelling (Louarn *et al.*, 2008*b*; Iandolino *et al.*, 2013). Such descriptions of canopy structures can then be combined with functional models in order to calculate, for each individual leaf, light interception (Mabrouk and Sinoquet, 1998; Louarn *et al.*, 2008*b*; Iandolino *et al.*, 2013), water status (Zhu *et al.*, 2017) or gas exchange (Prieto *et al.*, 2012). Leaf photosynthetic capacity, as estimated through parameters of Farquhar's model (Farquhar *et al.*, 1980) [i.e. maximal Rubisco carboxylation rate (V_{cmax}) and maximal electron transport rate (J_{max})] also varies with microclimate conditions within the canopy. Leaf N content and leaf mass per area (LMA) appeared to be good predictors of these variations for leaves at different positions within the canopy and during the growing season (Prieto *et al.*, 2012). For a given nutrition level, including the distribution of leaf N content in the canopy in the modelling can therefore account for spatial variation in photosynthetic capacity and represents an advantage compared with models using a spatially averaged, uniform N content (de Pury and Farquhar, 1997; Louarn *et al.*, 2015). In this study, we take into account the distribution of leaf N content and LMA within the canopy in order to upscale leaf photosynthesis and transpiration to the plant level in vines under different training systems.

The functional–structural plant model presented here extends the structural model TOPVINE (Louarn *et al.*, 2008*a*, *b*) by coupling with a leaf gas exchange module (Prieto *et al.*, 2012) to simulate whole-plant gas exchange. TOPVINE provides a set of 3D modelling tools based on an envelope-based approach to simulate canopy structure on different training systems. The objectives of this study were (1) to introduce the gas exchange model that was developed for the plant level based on leaf-level responses as influenced by 3D structure of the canopy, (2) to validate the model against an independent dataset recorded at the plant level over a wide range of canopy structures, and (3) to quantify the impact of the distribution of leaf N content within the canopy on gas exchange. The model developed and validated here provides a novel tool to estimate gas exchange at the canopy level, capturing the existing variability produced at the leaf level in grapevine canopy structure by the different training systems.

MATERIALS AND METHODS

Site description and plant material

The experiment was conducted during the 2009 season in a vineyard located at the SupAgro-INRA campus in Montpellier (43°37′ N, 3°52′ E), France. Grapevines 'Syrah' grafted onto SO4 were planted in 2000. Rows were oriented NW–SE at 140° from north. Measurements were performed on four different training systems. A low single-wire (LSW) system in which the canopy was free and shoots were not trained (Table 1, Fig. 1) was compared with three variations of vertically shoot-positioned (VSP) systems: low-density VSP with 3.6 m between rows (VSPl); high-density VSP with 1.8 m between rows (VSPh); and a low foliage-height version of VSPh with shoot trimming at 1.2 m (VSPh$_s$). Vine spacing was 1.0 m for all plots. Each plot consisted of three adjacent rows of 20 plants each. Measurements were performed on the central row.

All plants were spur-pruned on a bilateral Royat cordon, with six buds per square metre of soil. Vines were daily drip-irrigated and fertilized to ensure non-limiting water and nutrient conditions. Water applied was the same for all training systems and adjusted according to evapotranspiration and phenological stage. Predawn leaf water potential was regularly monitored throughout the season and never fell below −0.25 MPa.

Measurements of whole-plant gas exchange

Whole-plant gas exchange was measured with an open, portable gas exchange chamber system developed for grapevine as previously detailed (Perez Peña and Tarara, 2004). Briefly, the chamber consisted of a cylindrical aluminium frame, open at the top and closed at the bottom with polystyrene foam. The bottom foam isolated the chamber from the soil (Supplementary Data Fig. S1). Chambers were 1.20 m in diameter and 3 m in height (volume 3.36 m³). The covering plastic was a 35-μm-thick transparent polypropylene film (RXD32 Propafilm, Innovia Films, UK). The transmittance of the plastic between 400 and 1200 nm exceeded 95 % (measured with a spectroradiometer; FieldSpec® HandHeld Pro, Analytical Spectral Devices, USA). The photosynthetic photon flux density (PPFD; measured with a PAR Quantum sensor, Skye Instruments, UK) inside the chamber was >90 % of ambient PPFD (Supplementary Data Fig. S2).

The air supply was generated by a blower connected to each chamber, which aspirated the ambient air through a metal pipe (3 m in height) and uniformly directed it inside the chamber through holed plastic plenums placed on the foam floor. Air flow passing through the chamber was controlled with a butterfly valve installed between the blower and the chamber (Supplementary Data Fig. S1). To avoid increases in air temperature inside the chamber, the rate of air flow was set close to three chamber volumes per minute. The air flow rate was derived from continuous recording with a differential pressure transducer (PX170, Omega Engineering, UK) placed at the outlet of the blower. A reference method was also applied, consisting of measuring the time response of the outlet minus inlet CO_2 differential resulting from continuous CO_2 injection into the inlet air stream (Garcia *et al.*, 1990). If CO_2 is injected continuously into an open system, the CO_2 differential should exponentially approach a steady state with a time constant equal to the chamber volume divided by the volumetric air flow rate (Garcia *et al.*, 1990). This method was applied to each measured plant and a linear regression was established to convert the pressure-transducer signal into air flow rate for each measured vine (Supplementary Data Fig. S3). The mean air flow used during the whole season averaged 10.53 m³ min⁻¹, which corresponded to 3.13 times the volume of the chamber per minute.

The chamber operated as an open gas exchange system (Garcia *et al.*, 1990; Long *et al.*, 1996). Two chambers installed on two different plants with different training systems measured gas exchange simultaneously. Flowing air was continuously sampled at 1 L min⁻¹ with vacuum pumps (model EW-79600-04, Cole-Palmer, USA) installed at the inlet pipe and at the outlet of the chamber. Sampled air was driven through polyurethane pipes (6/4 mm diameter; Automacion Micromecanica, Argentina) to an infrared gas analyser (IRGA, CIRAS-2, PP

TABLE 1. *Planting distance, foliage height (H$_f$) and bud number for the different training systems used for model validation. Distance between plants within the row was 1 m for all training systems. 'Syrah', Montpellier, 2009*

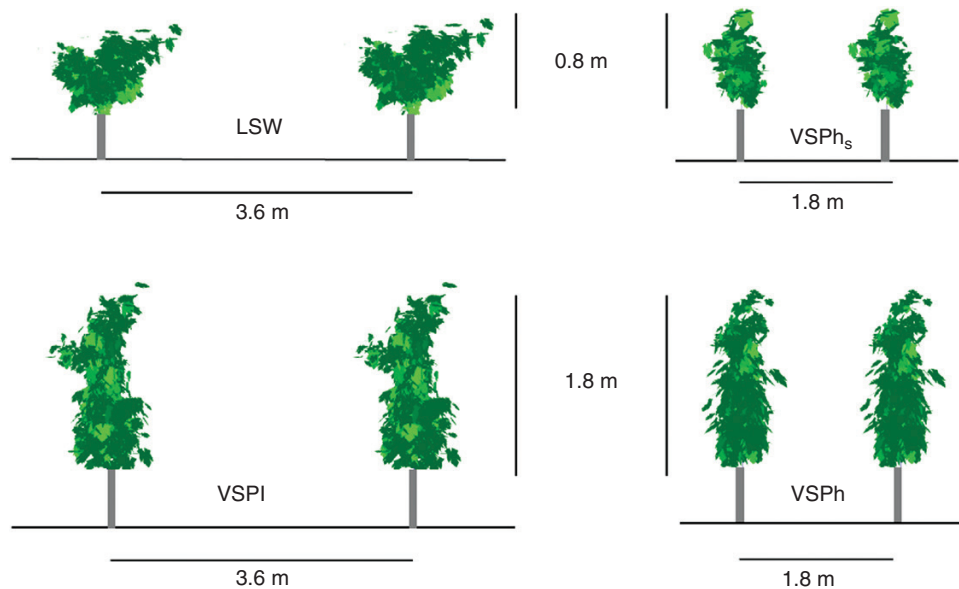|	LSW	VSPl	VSPh	VSPh$_s$
Distance between rows (m)	3.6	3.6	1.8	1.8
Vines per hectare	2777	2777	5555	5555
H$_f$ (m)	0.8	1.8	1.8	0.8
Buds per vine	24	24	12	12
Buds per square metre of soil	6	6	6	6

FIG. 1. Dimensions and distances between rows for the training systems used in model development and validation. Montpellier, 2009.

Systems, UK) working in differential mode. Air flow delivered to the IRGA was filtered (5 µm) and controlled to 0.20 L min^{-1} with a flowmeter. A manifold with solenoid valves (Serie 211 1/8″, Automacion Micromecanica, Argentina) was built in such a way that the two chambers were sampled alternately, each sampling period lasting 6 min. A data acquisition system driven by a datalogger (DT50 DataTaker, Victoria, Australia) was developed in order to control valve position, air sampling and data recording. For each chamber, gas exchange were calculated from sampled air analysis every 20 s, averaged for a 6-min period and recorded by the DT50 (120 values per plant per day). To avoid any drift between the reference and the analysis cells of the IRGA, two additional solenoid valves switched the air stream between the two cells at regular intervals (3 min), and the actual CO_2 and H_2O difference between the entry and the exit of the chamber was calculated as described by Garcia *et al.* (1994). This method avoided the need to set the zero manually and provided a fully automated system driven by the DT50 (Garcia *et al.*, 1994).

Canopy microclimate

Air temperature (T_{air}) and relative humidity (RH) inside the chamber were measured at canopy level (1.6 m) with a temperature and RH probe (HMP50, Campbell Scientific, UK) placed

on two ventilated radiation shields. Hygrometers were all calibrated at the beginning of the season (HG1 Optidew, Michell Instruments, UK). Leaf temperature (T_{leaf}) was measured on nine leaves per plant at different positions within the canopy (three inner leaves, three outer leaves on the east side and three outer leaves on the west side of the plant) with a thermocouple inserted in the main leaf vein on the abaxial, shaded face. The data obtained were used to build a regression between T_{leaf} and intercepted PPFD by the same leaves. Air temperature at the chamber inlet pipe was measured with a thermocouple placed inside the pipe after the blower. Measurements were recorded every 6 min by two dataloggers (CR10X and CR1000, Campbell Scientific, UK) equipped with two signal multiplexers (AM416 and AM16/32, Campbell Scientific, UK). The chamber increased air temperature at the canopy level by about 2 °C compared with ambient air during the afternoon (Supplementary Data Fig. S4). Night temperatures were similar between the outside and inside of the chamber. The rise in T_{air} in the chamber during the afternoon increased ambient vapour pressure deficit (VPD) by almost 1 kPa.

Stem heat balance sap flow

Sap-flow measurements were simultaneously performed on the same vines as those used for whole-vine gas exchange

measurements. Sap flow gauges (SGEX25, Dynamax, USA) operating with the heat balance method (Valancogne and Granier, 1991) were installed on the trunk at 0.30 m from the soil surface, avoiding nodes and irregular trunk sections and ensuring optimal contact between the sapwood and the heater and thermocouples. Gauges were double-wrapped with aluminium foil, which was extended to the soil to avoid an axial temperature gradient. Sensors were connected to a datalogger (CR1000, Campbell Scientific, UK) and a multiplexer (AM16/32, Campbell Scientific, UK). Heating was provided continuously by an external lead-acid battery branched to the gauges and the datalogger. Outputs were collected every 30 s, averaged and recorded every 6 min.

Acquisition of canopy 3D structure

After gas exchange and sap-flow measurements, vines were immediately digitized to capture the undistorted canopy architecture. The spatial coordinates of leaf blade bases, orientation angles and lengths of all leaves on each plant were recorded with an electromagnetic 3D digitizer coupled to a digitizing pen (Fastrak, Polhemus, Colchester, VT, USA). For each leaf, the pen was first placed in the blade at the petiole insertion point and then it was placed at the end of the main vein to record the leaf length. From these two measured points, the inclination and orientation angles were calculated for each leaf. Depending on the plant's size (between 700 and 900 leaves each), it took from 5 to 7 h to completely digitize one plant. Individual leaf areas were estimated through previously established allometric relationships for this variety between leaf length and its surface area (Louarn *et al.*, 2008*a*). We used this information to reconstruct virtual plots simulating the 3D canopy structure of each measured plant in the different training systems.

Meteorological data

Photosynthetic photon flux density (PAR Quantum sensor, Skye Instruments, UK), wind speed (A100R anemometer, Vector Instruments, UK), air temperature and RH (HMP45 AC, Campbell Scientific, UK) were measured at 3 m height in the middle of the plot. All sensors were connected to a datalogger (CR10X, Campbell Scientific, UK), and data were recorded every 6 min.

Data collection for model validation

In order to test the model against independent transpiration and photosynthesis data, whole-plant gas exchange chambers were installed on three plants per training system. These measurements were combined with sapflow sensors installed in the trunk to obtain a set of whole-plant transpiration dynamics for the different training systems during the season. Each series of measurements lasted for 3 d and consisted of monitoring whole-plant gas exchange, sap flow, microclimatic variables inside the chamber, and climatic conditions. Immediately after these measurements, the structure of each plant was completely digitized to record the 3D foliage characteristics as already described.

Model description

General overview. The model presented here calculates on an hourly time step the light interception and the gas exchange of a plant placed in the centre of a virtual scene. The model combines three components: (1) a module of 3D reconstruction of the plant canopy structure (Louarn *et al.*, 2008*b*); (2) a radiative transfer model (Chelle and Andrieu, 1998); and (3) a gas exchange model at the leaf level that takes into account the leaf N content and microclimate conditions as a function of leaf position in the canopy (Prieto *et al.*, 2012). A simple workflow was used to scale up photosynthesis and transpiration from a single leaf to the canopy (Fig. 2); LMA and leaf N content at a certain time during the season were related to PPFD intercepted by leaves during the 10 previous days ($PPFD_{10}$) and to cumulated thermal time (TT) as a proxy for the influence of leaf ageing (Prieto *et al.*, 2012). The leaf N content was used to calculate the parameters of the photosynthesis model (Farquhar *et al.*, 1980), through previously established regressions between leaf N content and Farquhar parameters (Prieto *et al.*, 2012). Finally, whole-plant photosynthesis and transpiration were calculated as the sums of the individual activities for each single leaf. Inputs to the model were climatic [day of the year (DOY), latitude, RH, PPFD, CO_2 concentration in ambient air] and microclimatic variables [RH_{ch} (relative humidity inside the whole-plant gas exchange chamber), T_{air}, T_{leaf}, $PPFD_{10}$, wind]. It must be pointed out that, excepting PPFD and T_{leaf}, the microclimatic variables (RH_{ch}, T_{air}, wind) were set equal for all leaves. The model was developed on the platform OpenAlea, an open-access platform for functional–structural plant modelling (Pradal *et al.*, 2008).

Reconstruction of 3D canopy structure

Canopy structures of plants measured with the whole-plant gas exchange chamber were completely digitized as described above. To create a complete plot, each digitized plant was replicated to create a 3D virtual plot consisting of three rows of three plants each. One file containing the *X*, *Y*, *Z* coordinates, leaf angles and sizes of all the leaves in the plants was used to build the virtual plot. To account for the impact of the chamber frame on light interception, an opaque structure representing the aluminium frame of the chamber was placed over the plant in the middle of the scene (Fig. 3).

Light interception model

Once the virtual plot was created, the radiative balance for each leaf of the scene was calculated with a radiative transfer model (CARIBU) based on the nested radiosity method (Chelle and Andrieu, 1998). The model deals with the direct light received by each surface and the scattered radiation from all the elements of the scene. To represent the diffuse radiation, we used a turtle-type discretization (Dauzat and Eroy, 1997) in which the sky hemisphere is divided into 46 zones using a standard overcast sky. The model was originally validated against Monte Carlo ray-tracing simulations (Chelle and Andrieu, 1998). In our study, light model
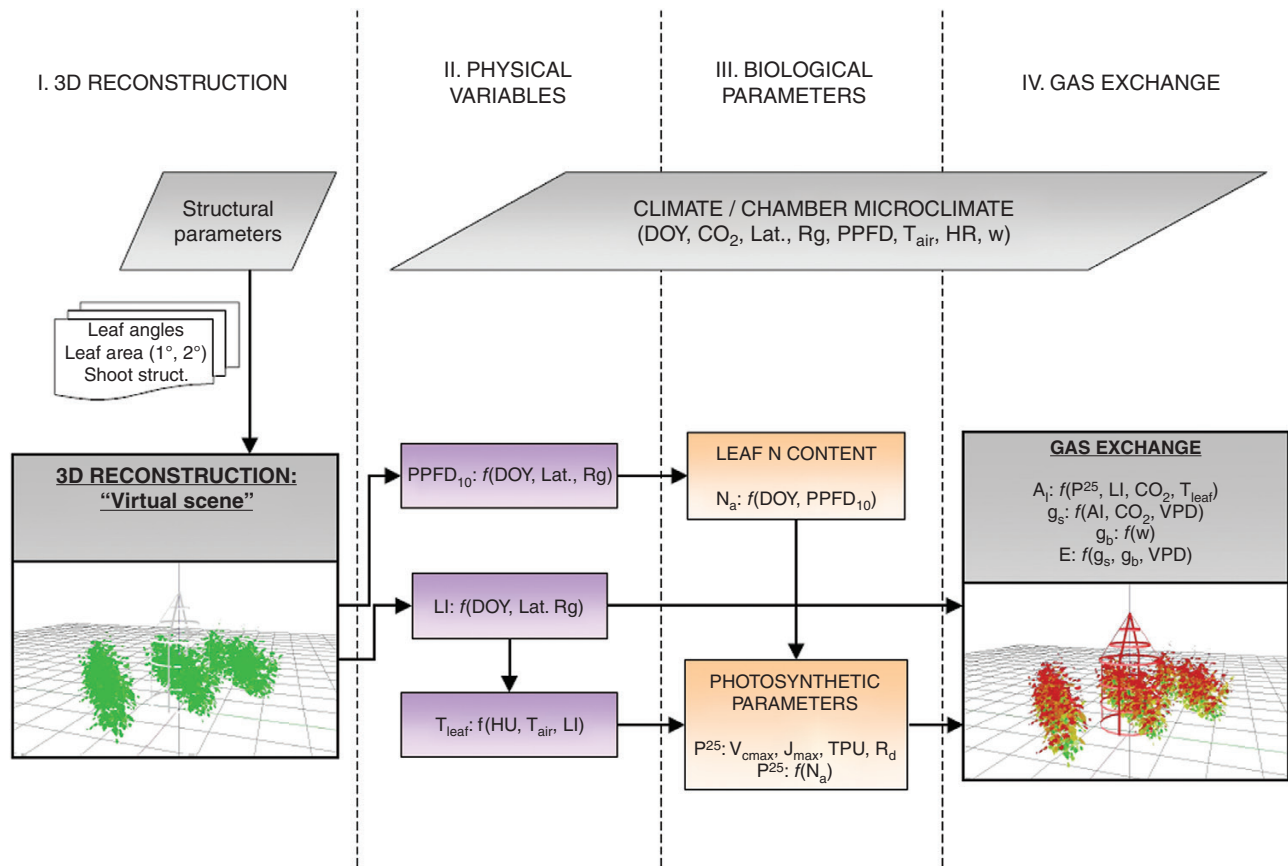
FIG. 2. Model structure. The model is divided into structural, physical and biological components and a gas exchange module. Inputs to the model are climatic and microclimatic variables (inside gas exchange chambers) and canopy structural parameters. The 3D reconstruction includes (I) the location, dimension and orientation of the leaves, which are combined with environmental conditions to calculate the microclimate variables (II), which are used in turn to estimate biological parameters (III) and ultimately to calculate gas exchange of each single leaf (IV). The microclimate of each leaf [leaf irradiance (LI), PPFD integrated over 10 d ($PPFD_{10}$) and T_{leaf}] are derived from a radiative transfer model (Chelle and Andrieu, 1998). Biological parameters include leaf nitrogen content (N_a), which is estimated with $PPFD_{10}$. The N_a is used to estimate the photosynthetic parameters at 25 °C (P^{25}) for each leaf [Rubisco maximal carboxylation efficiency (V_{cmax}), maximum electron transport rate (J_{max}), triose phosphate utilization (TPU) and dark respiration (R_d)]. Finally, physical, biological parameters and climatic and microclimatic variables are combined to estimate A_l (leaf net photosynthetic rate), g_s (stomatal conductance), g_b (boundary layer conductance) and E_l (leaf transpiration rate). For more details of the leaf model see Prieto *et al.* (2012). Canopy photosynthesis and transpiration are then integrated for all leaves in the plant. Environmental variables are: sun position calculated from time of day, day of the year (DOY) and latitude (lat), ambient CO_2 concentration (CO_2), global radiation (R_g), photosynthetic photon flux density (PPFD), air temperature (T_{air}), RH and wind speed (w).

output was compared with the experimentally determined intercepted light as a fraction of the incoming solar radiation intercepted by the canopy during a given period using hemispherical photographs (Louarn *et al.*, 2008*b*). Simulated and experimental daily fractions of intercepted light were highly correlated, with a root mean square error (RMSE) of 4 %, corresponding to ±2 mol m⁻² d⁻¹ (Supplementary Data Fig. S5).

Gas exchange model and photosynthetic capacity distribution within the canopy

Net carbon exchange, stomatal conductance and transpiration rate were calculated for each leaf in the plant using a biochemical model of photosynthesis (Farquhar *et al.*, 1980) coupled to a stomatal conductance model (Leuning, 1995). The complete leaf model was described and validated at the leaf scale in a previous work (Prieto *et al.*, 2012). In summary, we considered that leaf photosynthetic capacity distribution within the grapevine

canopy is driven by the acclimation of leaves to $PPFD_{10}$. For this, once the 3D mock-up was created, CARIBU was run over the 10 preceding days in the whole-plant chamber to calculate $PPFD_{10}$ (mol m⁻² d⁻¹) of each leaf as a proxy of leaf acclimation. $PPFD_{10}$ was then used to compute LMA for each leaf:

$$\text{LMA} \left(\text{g cm}^{-2} \right) = a_M \cdot \ln \left(PPFD_{10} \right) + b_M \qquad (1)$$

Leaf N content on a mass basis (N_m) was calculated as a function of thermal time since bud burst (TT) as a proxy for the effect of leaf ageing on N content, and used to calculate N content per unit area (N_a):

$$N_m \left(\% \right) = a_N TT + b_N \qquad (2)$$

$$N_a \left(\text{g cm}^{-2} \right) = \text{LMA } N_m \qquad (3)$$

where a_M, b_M, a_N and b_N are mean, fitted coefficients valid for all leaves (Prieto *et al.*, 2012). Once N_a was calculated, the photosynthetic capacity of each leaf was estimated through
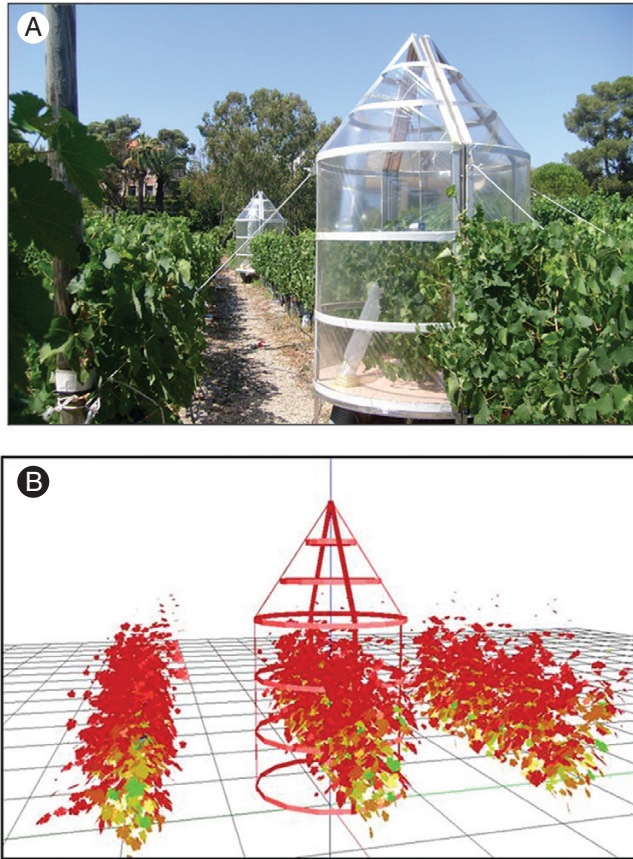
Fig. 3. (A) View of the experimental plot, including the whole-plant gas exchange chamber. (B) A 3D reproduction of the plot, including a virtual whole-plant gas exchange chamber to account for the effects of the aluminium frame on light interception.

previously established linear regressions between N_a and photosynthetic parameters:

$$P^{25} = S_{Na}N_a + b_{Na} \qquad (4)$$

where P^{25} is the value of V_{cmax}, J_{max}, triose phosphate utilization (TPU) or dark respiration (R_d) at 25 °C, and S_{Na} and b_{Na} are the slope and intercept of the relationship, respectively. Our approach considered a mean age for the leaves (for a given phenological stage) in the plant, and did not discriminate between primary and lateral leaves. The outputs of the model were intercepted light (PPFD$_i$), net CO_2 exchange (NCE) and transpiration (Tr) rate, expressed per plant or per square metre of soil.

Leaf temperature and boundary layer conductance

Leaf temperature was calculated through a statistical approach. For each hour of the day (from 0400 to 2000 h) a linear relationship between the PPFD intercepted by the leaf and the difference between the air and the leaf temperatures ($\Delta T_{leaf–air}$) was used to calculate T_{leaf}.

$$\Delta T_{leaf−air} = a\, PPFD + b \qquad (5)$$

The relationships between $\Delta T_{leaf−air}$ and PPFD were established from a dataset of around 100 leaves with different positions

within the canopy measured during several days. Since a uniform wind speed inside the canopy was produced with the whole-plant chamber (Garcia *et al.*, 1990), we considered a unique mean boundary layer conductance (g_b) for all leaves (2.357 mol m$^{−2}$ s$^{−1}$; Prieto *et al.*, 2012).

Impact of leaf N distribution on simulated gas exchange

The model presented here is based on the observed responses of leaf traits to irradiance and on effects of N_a on photosynthetic capacity. The model considers that exposed leaves have a higher N_a than inner leaves, favouring photosynthesis in exposed leaves. In order to assess the advantage of using the empirical–observed distribution compared with a uniform N_a content, a sensitivity analysis was performed considering two theoretical cases. First, for a single plant we selected the leaf with the highest N_a and applied it to all the leaves, thereby maximizing the photosynthetic capacity of the plant corresponding to all leaves considered as sunlit without limitation by N redistribution (N_{unlim}). Second, we used the model to estimate the total N content of the same plant and then we distributed it homogeneously on all the leaves considering that all leaves in the plant equally shared a common and limited pool of N (N_{lim}). Although both distributions were uniform, they represented two different, extreme theoretical cases. The simulations were run on two plants on different training systems (LSW and VSPh$_s$).

Evaluation of model performance

Model simulations were compared with a dataset of 25 different situations (training systems and environmental conditions) recorded during the 2009 season. The data for validation covered a wide range of environmental conditions (Table 2). Model performance was evaluated through the RMSE calculated for assimilated CO_2 and transpiration (1) on an hourly time step and (2) integrating the values during a whole day:

$$RMSE = \sqrt{\frac{\sum\limits_{i=1}^{n} (P_i - O_i)^2}{n}}$$

where P_i and O_i are the predicted and observed values, respectively, and n is the number of individual values. We also calculated the model agreement index (d, Willmott, 1982):

$$d = 1 - \frac{\sum\limits_{i=1}^{n} (P_i - O_i)^2}{\sum\limits_{i=1}^{n} \left(|P_i - \bar{O}_i| + |O_i - \bar{O}_i|\right)^2}$$

where $\bar{O}_i$ is the mean observed value. This index ranges between 0 and 1, with 1 indicating perfect agreement between simulated and observed values.

RESULTS

Meteorological conditions

Measurements were performed during two periods in the 2009 season: bunch closure, from 20 June to 6 July (DOY 171–188);

TABLE 2. *Environmental conditions during measurements.* T$_{min}$, T$_{max}$, *VPD$_{min}$ and VPD$_{max}$ are the minimal and maximal values of temperature and VPD inside the chambers at the canopy level,* T$_{air}$ *is the mean air ambient temperature, and cumulated PPFD is the incident radiation integrated over the whole day. 'Syrah', Montpellier, 2009*

Phenological stage	Daily temperature (°C)			Daily VPD (kPa)			Cumulated PPFD (mol m^{-2} d^{-1})	
	T_{air}	T_{max}	T_{min}	VPD$_{mean}$	VPD$_{max}$	VPD$_{min}$	PPFD$_{max}$	PPFD$_{min}$
Bunch closure	25.1 ± 2.5	32.9 ± 2.8	19.8 ± 2.6	2.1 ± 0.3	3.6 ± 0.6	0.6 ± 0.2	59.9	39.2
Veraison	24.9 ± 1.7	33.9 ± 2.4	18.7 ± 1.7	2.1 ± 0.5	3.7 ± 0.9	0.5 ± 0.2	54.6	34.1

and from veraison to the beginning of ripening, from 27 July 2009 to 14 August 2009 (DOY 208–226). The meteorological conditions were quite similar during the two periods (Table 2), with, on average, daily mean and maximal (T_{max}) temperatures of 25 and 33 °C, respectively, and with some days when T_{max} exceeded 36 °C. Maximum VPD ranged from 2.2 to 5.7 kPa. Daily maximum VPD averaged over the two periods was 3.6 kPa. Average daily cumulated PPFD in the two periods indicated prevailing sunny conditions. These environmental conditions are commonly observed in Mediterranean and arid wine-growing regions.

Model validation

The model was validated over 25 d on the four trellis systems for NCE and over 15 d for transpiration rate on two different trellis systems (VSPl and VSPh$_s$). We validated transpiration rate against sap-flow values since the corresponding dataset was larger than with whole-plant chambers.

NCE

A representative daily dynamic of light interception, microclimatic conditions inside the whole-plant chambers, measured and simulated values of NCE are presented for each training system (Fig. 4). For each measured plant, the daily course of NCE was measured with a time step of 12 min (120 points per plant per day). Due to row orientation, higher light interception was observed during the afternoon for all systems, but this did not entail a higher photosynthesis rate. The NCE reached its maximum between 1000 and 1200 h and stayed at similar values until ~1600 h. However, a slight decrease in NCE was observed on some days around midday; this was clearly observed for VSPl and less clearly for LSW, which were both measured during DOY 171 (Fig. 4K, L). In spite of substantial variation in environmental conditions during both periods, daily integrated NCE per plant (NCE$_{dpl}$) closely correlated with total leaf area (TLA) and leaf area index (LAI) (data not shown). Accordingly, the highest instantaneous NCE per plant (NCE$_{pl}$) was observed on the VSPl vines (around 70 µmol plant^{-1} s^{-1} at berry set) due to their higher TLA, followed by VSPh (45 µmol plant^{-1} s^{-1}), whereas LSW and VSPh$_s$ presented smaller maximum assimilation rates (around 36 µmol plant^{-1} s^{-1}). When expressed per square metre of soil (NCE$_s$), the highest assimilation rates were observed for VSPh (between 20 and 25 µmol m^{-2} s^{-1}), followed by VSPh$_s$ and VSPl (between 15 and 20 µmol m^{-2} s^{-1}), whereas LSW presented the lowest NCE$_s$ (10 µmol m^{-2} s^{-1}).

Overall, the model accurately simulated the daily pattern of NCE$_{pl}$ for the different training systems. The model showed low RMSE of between 1.51 and 4.73 and an agreement index (*d*) between 0.92 and 0.97 for the four systems studied (Table 3). However, a systematic underestimation appeared, especially at high NCE values (Fig. 5A). Although the global RMSE was low, it presented a systematic error of 25 % (Table 3). For LSW and VSPh$_s$, the model showed a low RMSE, high *d* and a small systematic component of RMSE (RMSE$_s$; 10 % for VSPh$_s$ and 23 % for LSW) in most situations where these systems were simulated. Even if the model performed well for VSPl (small RMSE and high *d*), a constant underestimation around 2.5 µmol m^{-2} s^{-1} was observed over nearly all of the day. The model was less accurate for VSPh, where we observed the highest RMSE (4.73), a RMSE$_s$ of 50 % and a mean bias error (MBE) during the morning around 7 µmol m^{-2} s^{-1} (Fig. 4M). This systematic underestimation of NCE in VSPh was observed during the morning and until midday; thereafter the error was randomly distributed. The final performance of the model, combining all the data for all the training systems, presented high values of the agreement index and low error estimates (Fig. 6A). Furthermore, when analysing the daily integrated CO$_2$ exchange (NCE$_{ds}$) for all the dataset, the model still showed good performance (Fig. 6B, Table 3). The RMSE remained very low (0.09 mol m^{-2} d^{-1}) and *d* was high (0.84).

Plant transpiration rate

Transpiration rate was measured simultaneously with sap-flow gauges installed in the trunk and with whole-plant gas chambers. On the one hand, these two independent methods could be compared, and on the other hand the sap-flow gauge method expanded the available dataset to validate the model. A good correlation was observed between transpiration measured with the chambers and that measured with the sap-flow gauges (r^2 = 0.85, slope not different from 1; Supplementary Data Fig. S6). Overall, both methods provided reliable values that were within the same range. Daily water use (Tr$_{pl}$) ranged between 2 and 6 L plant^{-1} day^{-1} for the different training systems depending on weather conditions. For one single plant, Tr$_{pl}$ was more variable than NCE from one day to another. A close relationship between daily integrated Tr$_{pl}$ and VPD$_{max}$ was observed. During a 10-d period, Tr$_{pl}$ ranged from 3.6 L plant^{-1} d^{-1} at 2.5 kPa VPD$_{max}$ to 6.4 L plant^{-1} d^{-1} at 4.7 kPa VPD$_{max}$, showing a high dependency of water use on environmental conditions.
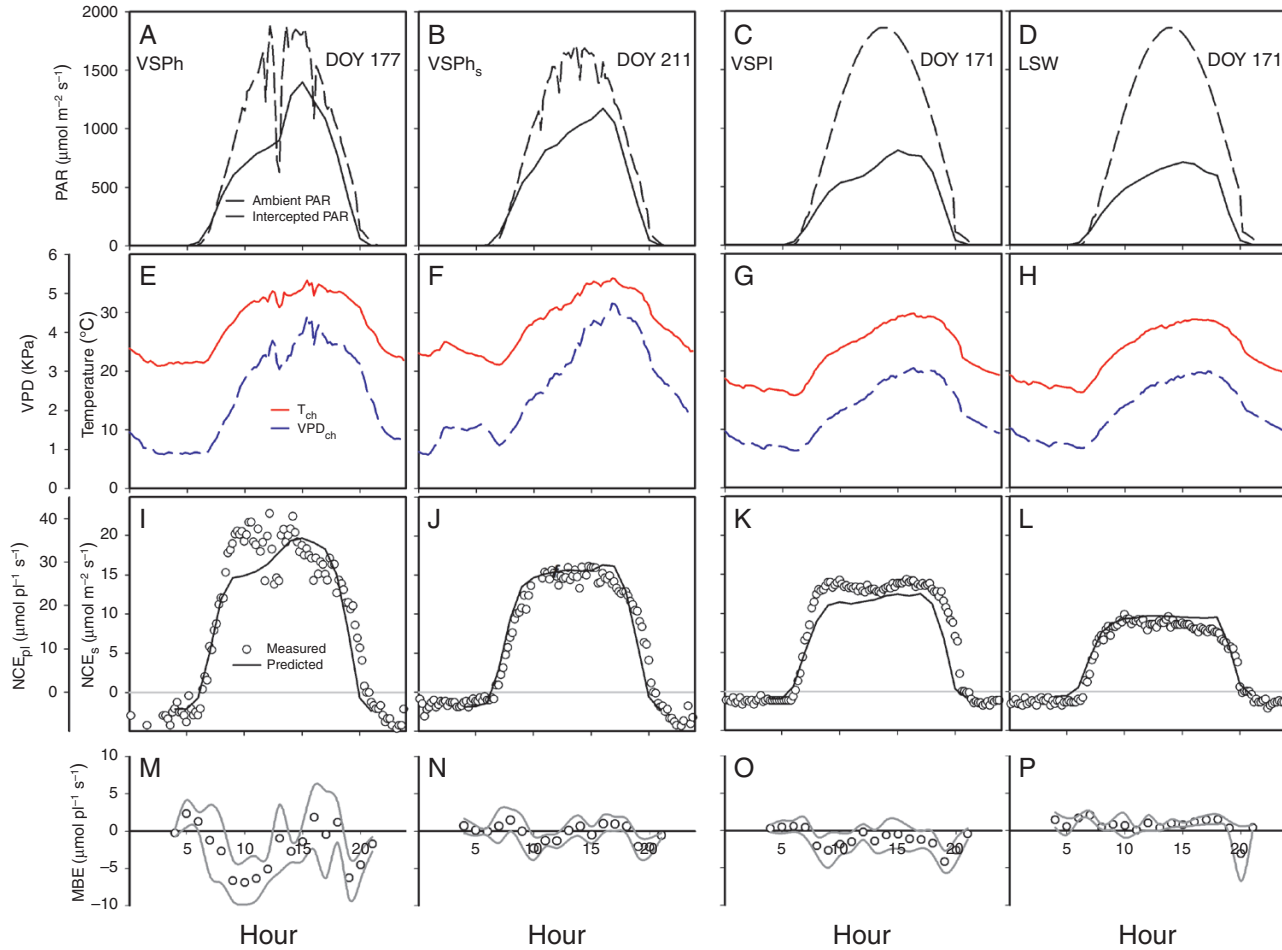
FIG. 4. Comparison between measured values and model predictions. Daily course of ambient and simulated intercepted PAR (A, B, C, D); chamber temperature and VPD (E, F, G, H); measured and predicted NCE (I, J, K, L) per square metre of soil (NCE_s) and per plant (NCE_{pl}); and mean bias error (MBE; M, N, O, P) for each trellis system. Measurements were performed on DOY 177 for VSPh (A, E, I, M), DOY 211 for $VSPh_s$ (B, F, J, N), and DOY 171 for both VSPl (C, G, K, O) and LSW (D, H, L, P). MBE was calculated for the whole dataset measured on each trellis system during the whole season, and not for the single day shown. Solid lines in (I), (J), (K) and (L) correspond to model predictions. Solid grey lines in (M), (N), (O) and (P) show the confidence intervals of MBE at $P = 0.05$. Montpellier, 2009.

TABLE 3. *Evaluation of NCE predictions for each of the training systems. Values of RMSE, the percentage corresponding to a systematic error ($RMSE_s$), a randomly distributed error ($RMSE_u$), index of agreement (d) and the slope and intercept of the regression between observed and predicted were calculated on an hourly basis. The same indexes were calculated for the daily integrated values ($Daily_{total}$).* 'Syrah', Montpellier 2009

	RMSE	$RMSE_s$	$RMSE_u$	*d*	Slope	Intercept
VSPl	2.58	48 %	52 %	0.94	0.77	0.60
$VSPh_s$	2.50	10 %	90 %	0.97	0.89	0.74
VSPh	4.73	49 %	51 %	0.92	0.76	0.49
LSW	1.51	23 %	77 %	0.97	0.94	0.99
Total*	**2.80**	**25 %**	**75 %**	**0.95**	**0.82**	**0.84**
$Daily_{total}$[†]	**0.09**	**48 %**	**52 %**	**0.84**	**0.51**	**0.22**

*N_{total}: 445 points. The hourly RMSE is in µmol m^{-2} s^{-1}.

[†]N_{daily}: 25 d. The daily RMSE is in mol m^{-2} d^{-1}.

An example of model simulations for Tr is presented for a 10-d measurement period in the $VSPh_s$ (Fig. 6). The model accurately simulated the pattern of Tr_{pl} over different environmental conditions and performed equally well in the two training systems (Table 4). The predicted values of the model showed an RMSE of 0.55, index *d* of 0.97 and an $RMSE_s$ of 19 %. Simulations were also close to the hourly transpiration observed (Fig. 7A), with an RMSE <1 mmol m^{-2} s^{-1}. The
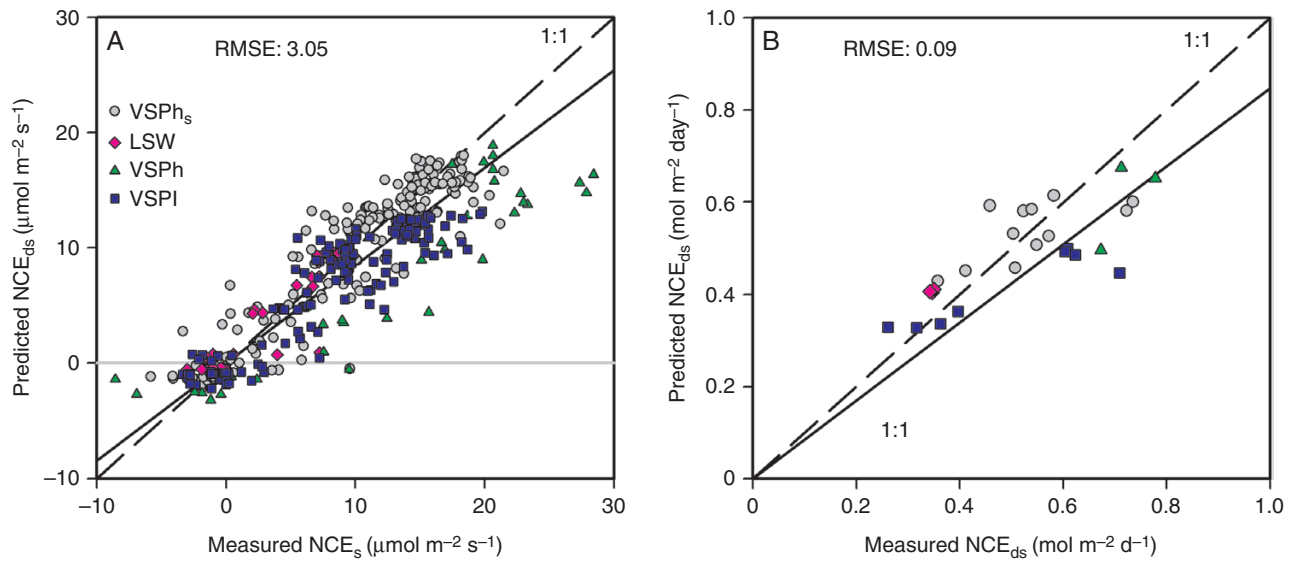
FIG. 5. Comparison of measured and predicted values of NCE per square metre of soil (NCE$_s$) on an hourly basis (A) and integrated for the whole day (NCE$_{ds}$) (B). Data correspond to the four trellis systems recorded over 24 different days. The solid line is the fitting for all data and the dashed line represents the 1 to 1 relation. Montpellier, 2009.
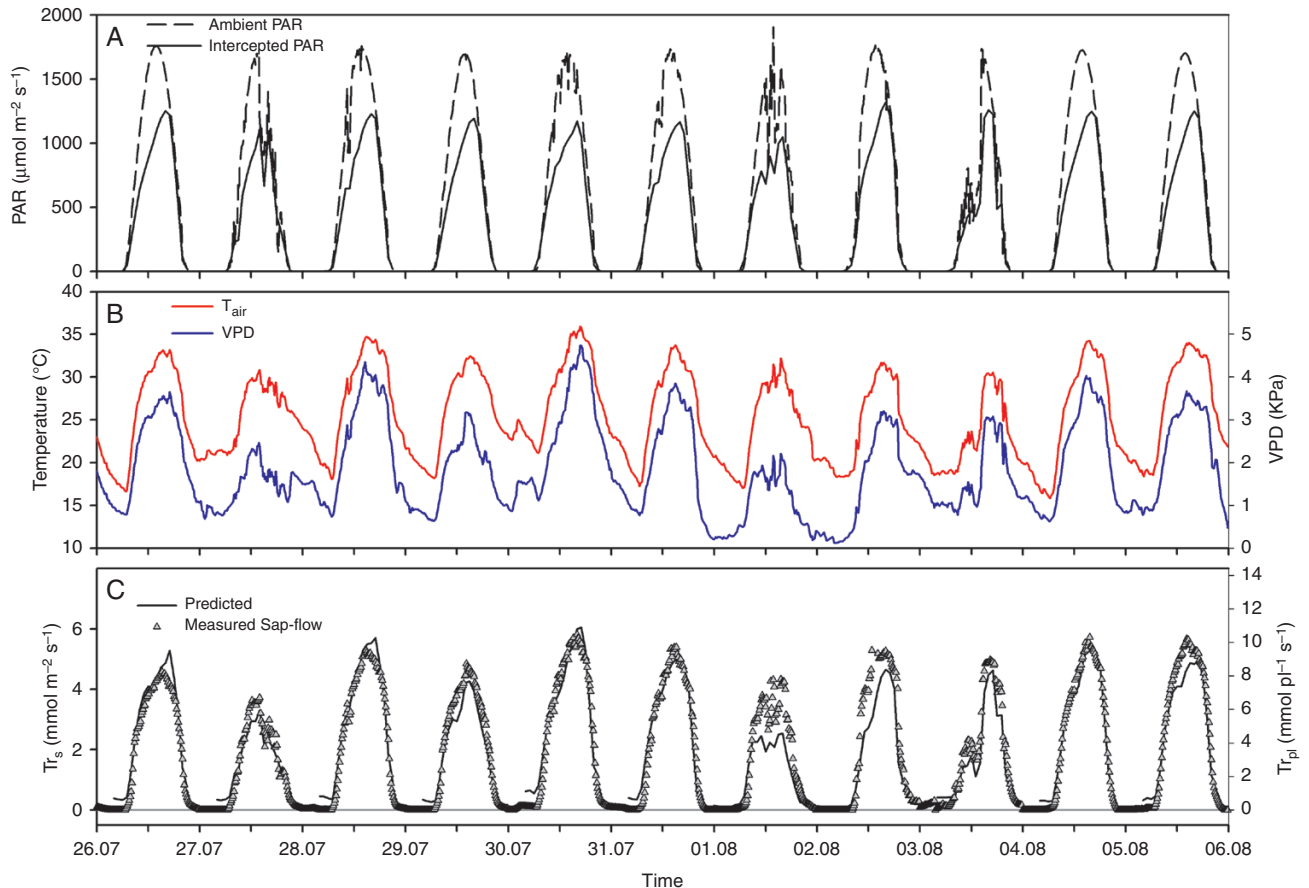

FIG. 6. Comparison between measured values and model predictions. Daily course of ambient and intercepted PAR (A), air temperature and VPD (B), and measured and predicted net transpiration rate per square metre of soil (Tr$_s$) and plant (Tr$_{pl}$) (C). The solid line in (C) corresponds to model predictions. Measurements of sap flow were performed on VSPhs on the same plant as that shown in Fig. 4B. Data from DOY 207–217. Montpellier, 2009.

TABLE 4. *Evaluation of transpiration (Tr) predictions for each raining system[1], 'Syrah'. RMSE, percentage corresponding to systematic error (RMSE$_s$), randomly distributed error (RMSE$_u$), index of agreement (d) and the slope and intercept of the regression between observed and predicted were calculated on an hourly basis. The same indexes were calculated for the daily integrated values (Daily$_{total}$). Montpellier, 2009*

	RMSE	RMSE$_s$	RMSE$_u$	d	Slope	Intercept
VSPl	0.33	11 %	89 %	0.94	0.86	0.06
VSPh$_s$	0.61	26 %	74 %	0.97	0.85	0.22
Total*	**0.55**	**19 %**	**81 %**	**0.97**	**0.86**	**0.15**
Daily$_{total}$[†]	**40**	**24 %**	**76 %**	**0.92**	**1.13**	**−53**

*N_{total}: 269 points. The hourly RMSE units are in mmol m^{-2} s^{-1}.

[†]N_{daily}: 15 d. The daily RMSE units are in mol m^{-2} d^{-1}.

agreement index (*d*) indicated >90 % agreement between observed and simulated values of daily integrated transpiration (Tr$_{ds}$; Fig. 7B). The RMSE was 40 mol m^{-2} d^{-1}, which represents around 10 % of total daily water use.

Impact of N distribution on simulated gas exchange

In order to explore the impact of N distribution within the canopy, we evaluated two alternatives: an unlimited N distribution (N_{unlim}) maximizing canopy photosynthesis, and a limited one (N_{lim}) corresponding to uniform reallocation of the total amount of N contained in all leaves of the plant as determined by the model. Simulations showed that the non-limiting distribution (N_{unlim}) overestimated the measured NCE$_{dpl}$ by 28 %, whereas the limited distribution (N_{lim}) underestimated NCE$_{dpl}$ by 18 % (Fig. 8). When comparing measured and predicted values on an hourly basis, the systematic error associated with N_{unlim} and N_{lim} was 51 and 53 % of the RMSE, respectively, which are high percentages compared with the 25 % RMSE observed with the original model (Table 3). Furthermore, the RMSE$_s$ of the daily integrated values was almost 98 % of the total error, more than 2-fold the RMSE$_s$ observed for the optimal distribution (Table 3, Daily$_{total}$). Nitrogen use efficiency (NUE) was calculated as the ratio between total C assimilated during the day and the total amount of N per plant (Ripullone *et al.*, 2003). The results showed that NUE was higher with the non-uniform distribution (4.9 gC gN^{-1} for VSPh$_s$ and 7.90 gC gN^{-1} for LSW) and lowest for the N_{unlim} distribution, whereas the distribution N_{lim} presented intermediate values.

DISCUSSION

Our results show that the model accurately reproduced grapevine canopy gas exchange under different training systems, providing a novel tool to evaluate the effects of canopy structure on whole-plant behaviour. In our model, the responses of individual leaves are integrated to reproduce the response of the whole canopy by coupling different tools, comprising (1) a detailed 3D description of the foliage architecture to estimate irradiance at each individual leaf; (2) the spatial and temporal variability of light interception and leaf photosynthesis; and (3) net CO$_2$ and H$_2$O canopy fluxes calculated as a function of leaf irradiance, leaf temperature and VPD.

Measured whole-plant NCE and transpiration

Functional–stuctural plant models are increasingly being used to understand complex interactions between plant architecture and physiological processes in many species at different scales. However, it is necessary to obtain experimental evidence that the model mimics the simulated processes (Wang *et al.*, 2018). Therefore, a key challenge when working with models at the plant scale is their validation with independent field data, specially for fruit perennials. Yet very few attemps have been performed to validate gas exchange models at the plant scale. Validations have only been performed at the branch scale in walnut (Le Roux *et al.*, 1999; Sinoquet *et al.*, 2001), apples (Massonnet et al., 2008) and coffee (Dauzat *et al.*, 2001, although only for transpiration using sap-flow gauges). Here we developed an automatic system to record whole-plant gas exchange in the field and combined with sap-flow gauges installed on the trunk of the same vine. Vine size varies considerably (TLA ranged from 3.0 to 7.8 m^2 in our experiments), with a major impact on net CO$_2$ exchanges. Our values of NCE integrated over the day (NCE$_{dpl}$) ranged from 97 g CO$_2$ plant^{-1} d^{-1} (around 7.8 m^2 of TLA) for VSPl to 37 g CO$_2$ plant^{-1} d^{-1} for VSPh$_s$ (3.0 m^2). If these values were expressed per square metre of soil (NCE$_s$), the highest values were observed in the high-density systems VSPh and VSPh$_s$ (around 32 g CO$_2$ m^{-2} d^{-1}). When expressing NCE per square metre of leaf area, the values ranged from 5 to 10 µmol m^{-2} s^{-1}, similar to other studies (Intrieri *et al.*, 1997; Intrigiolo and Lakso, 2011; Tarara *et al.*, 2011; Merli *et al.*, 2015).

Water use varied from 2 to 6 L plant^{-1} d^{-1} depending on environmental conditions and plant size. The range of water use observed here is very similar to that reported by Braun and Schmid (1999) for Chardonnay, and Poni *et al.* (2014*a*) for Sangiovesse. However, it is much smaller than those reported in other studies (Williams and Ayars, 2005; Dragoni *et al.*, 2006; Tarara and Perez Peña, 2015). These differences are primarily explained by higher TLA per plant in these other studies (around 25 m^2).

Model performance as regards whole-plant gas exchange

One of the main objectives of the study was to evaluate the model performance with a large variety of canopy architectures. For this, we evaluated the accuracy of model predictions against
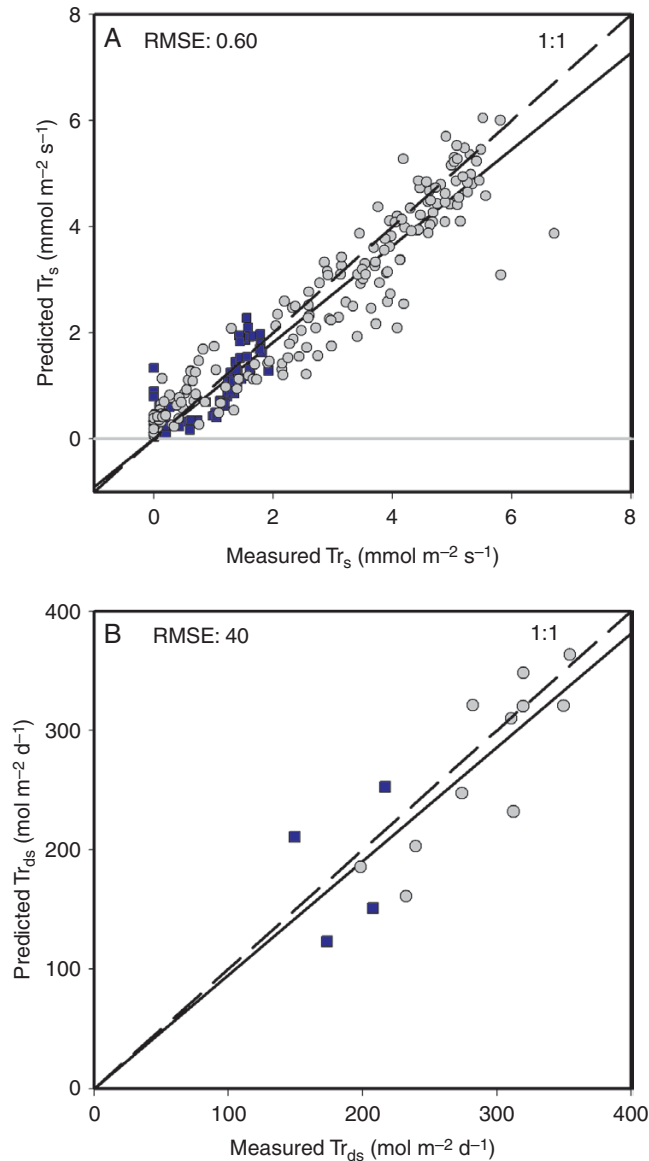
FIG. 7. Comparison of measured and predicted values of transpiration rate per square metre of soil (Tr_s) on an hourly basis (A) and integrated for the whole day (Tr_{ds}; B). Model output is compared with values measured with the sap-flow gauges. Data correspond to two trellis systems over 15 d. Blue squares, VSPl; grey circles, VSPh$_s$. The solid line is the fitting for all data and the dashed line represents the 1 to 1 relation. Montpellier, 2009.

FIG. 8. Measured and predicted values of NCE per square metre of soil (NCE$_s$) and per plant (NCE$_{pl}$) for two plants. (A) VSPh$_s$. (B) LSW. The model was run as originally conceived (solid black line) and with different N distributions within the plant: N_{unif} (red line), where a maximal non-limiting N_a value was applied for all leaves in the plant, and N_{lim} (blue line), where a uniform N_a value was applied for all leaves, limited by the total amount of N predicted from Prieto *et al.* (2012) within the whole plant.

a dataset of whole-plant gas exchange recorded in a set of contrasting canopy architectures. Although it is time-consuming to digitize a whole plant, by recording the exact position and orientation of all leaves the accurate 3D canopy representation obtained makes it possible to compare the model outputs directly with the measured plant without being dependent on the quality of plant architecture simulation (Dauzat *et al.*, 2001).

Our model accurately followed the daily pattern of photosynthesis and transpiration rates for the simulated training systems. Instantaneous values of NCE and Tr (per soil or plant) were predicted with <10 % RMSE for all systems except for VSPh (RMSE 18 %), similar to the error found in other studies
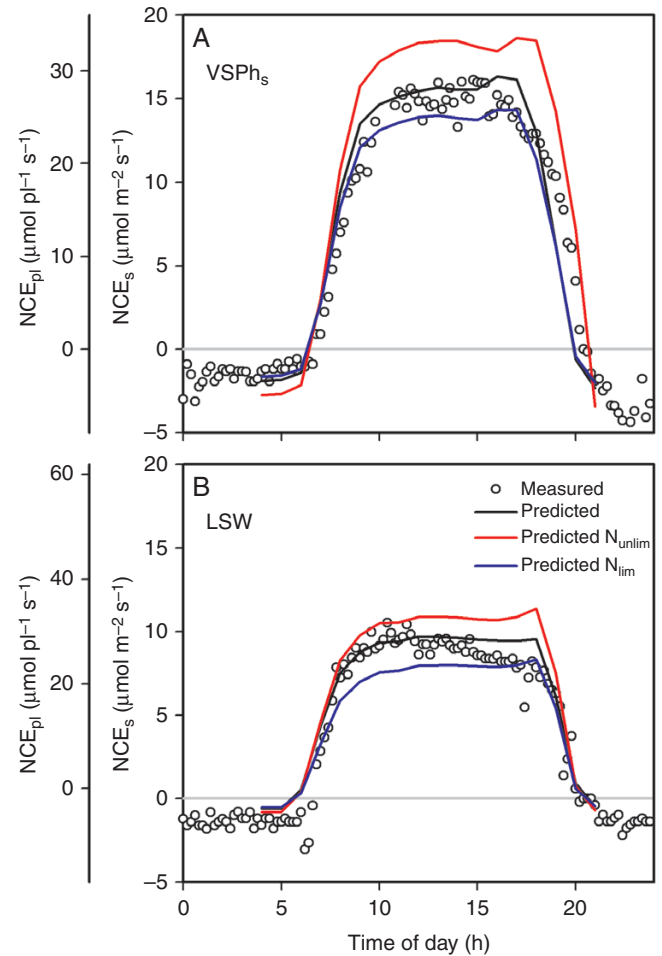
(Le Roux *et al.*, 1999; Sinoquet *et al.*, 2001; Massonnet *et al.*, 2008). The index *d* indicated between 92 and 97 % agreement between measured and predicted values for each system considered individually and 95 % for all systems together.

Our modelling approach implies two main assumptions: (1) the spatial distribution of photosynthetic capacity (V_{cmax}, J_{max}) within the canopy, is driven by leaf acclimation (through changes in LMA and N_a) to light interception over the 10 previous days (Prieto *et al.*, 2012); and (2) total plant net C assimilation and transpiration is the sum of the activity of each single leaf on the plant (it does not include respiration or water used by other organs, such as shoots and grapes). Accounting for the distribution profile of N content within the canopy allowed us to calculate V_{cmax}, J_{max} and R_d for each single leaf in the canopy. In a first step, we used a time-cumulation of irradiance during previous 10 d (PPFD$_{10}$) to assess individual leaf N content and its photosynthetic capacity. Accounting for this middle-term leaf acclimation to intercepted light is a realistic approach since N content can be redistributed in a canopy over a period of

several days, but cannot adjust on shorter time-scales associated with the movement of the sun during the day (de Pury and Farquhar, 1997). Second, we used instantaneous environmental and microclimatic conditions as input to simulate gas exchange, which accounted for transient environmental changes during the day. Other studies, instead of considering leaf trait acclimation to light in order to predict effects on photosynthetic capacity, directly considered different responses of photosynthesis to light for leaves with different exposures to radiation (Sarlikioti *et al.*, 2011; Poirier-Pocovi *et al.*, 2018; Rakocevic *et al.*, 2018; Chang *et al.*, 2019). In this study, we followed a more mechanistic approach, explicitly outlining the temporal and spatial leaf acclimation to intercepted light through structural (LMA) and functional (N_a) traits separately. The time step of the model was 1 h, and we were not able to account for very rapid microclimatic changes such as sun flecks (Kriedemann, 1968). However, in simulations performed on days with changing environmental conditions, the model reproduced accurately the pattern induced by fluctuating radiation, temperature or humidity. Decreasing the time step would increase the calculation time, limiting the number of cases that could be studied. The approach that was successfully applied here suggests that in non-limiting water conditions canopy functioning results from the addition of the activities of individual leaves acclimated to the radiation regime cumulated over the past 10 d.

Considering possible constraints on leaf N content when scaling up from leaf to canopy

The N distribution within a canopy has usually been analysed using optimization theory (Field, 1983). This means that, for a given plant, N is optimally distributed if any re-allocation of N within the canopy decreases the photosynthetic rate. Therefore, more N is expected to be allocated in the most exposed leaves and less in the shaded ones (Hirose and Werger, 1987). However, optimal theory does not provide the mechanisms explaining the distribution of resources within a plant (Kull and Jarvis, 1995; Kull and Kruijt, 1998, 1999). Furthermore, several studies demonstrate that the distribution is close to, but not really optimal (Leuning *et al.*, 1995; Niinemets and Tenhunen, 1997; de Pury and Farquhar, 1997). Leaves are subjected to unpredictable and changing environmental conditions, and given that plants have to deal with other limiting factors (wind, temperature, herbivory) it seems reasonable that full acclimation to one single environmental condition does not occur (Niinemets and Anten, 2009).

In order to evaluate the effects on NCE_{pl} of distributing N within the canopy, we performed two simulations with different distributions. We applied a non-limiting N content for all leaves in the canopy (N_{unlim}) in order to maximize individual leaf photosynthetic capacity, and second, based on the total amount of N in leaves calculated for a whole plant, a limited, uniform amount of N was equally set for each leaf (N_{lim}). The results of the first distribution (N_{unlim}) showed that NCE_{pl} was overestimated by almost 28 %. This result confirms that using the photosynthetic capacity of sun-exposed leaves to represent all the leaves in canopies growing under high incident light overestimates NCE (Sarlikioti *et al.*, 2011), in our case

by 28 %. Most of the actual knowledge produced in the last 20 years is at the leaf scale (Kull and Kruijt, 1999), and most studies on grapevine were performed on fully exposed leaves. Extrapolating such leaf-level data to the whole canopy can lead to misleading results (Poni *et al.*, 2014*b*; Merli *et al.*, 2015). The results for the limiting distribution (N_{lim}) showed that NCE_{pl} was underestimated by 18 %. Similar trends were observed in several studies, with the magnitude of the difference between a uniform and the actual distribution being dependent on the species, water status, nutrition and LAI (Hirose and Werger, 1987; Leuning *et al.*, 1995; Sinoquet *et al.*, 2001; Sarlikioti *et al.*, 2011). Leaves of the same plant are not independent of each other and share a common limiting pool of resources (Kull and Kruijt, 1999). In our case, the observed N distribution profile shows that the common limiting pool of resources was distributed in order to improve plant C gain. The differences observed between the different N distributions demonstrate the importance of considering a detailed prediction of N distribution based on appropriate description of canopy structure with calculation of light distribution within canopy.

Model limits

We assumed that T_{air}, RH, wind speed (w) and CO_2 were uniform within the canopy. Thus, a unique g_b was calculated for all the leaves based on mean air flow through the chamber. Considering that air flow inside the chamber was set to a relatively high value to get uniform conditions for correct operation (Garcia *et al.*, 1990), so that g_b can be approximated by considering w equal to the air-flow rate inside the chambers (Müller *et al.*, 2008), the approach taken here appears acceptable. By contrast, in field conditions g_b is highly variable, depending on leaf position within the canopy, row orientation, wind speed and direction, and canopy density (Daudet *et al.*, 1998). However, data concerning wind variability within different canopy structures on grapevine are scarce and should be addressed in more detail for different training systems under natural wind conditions (Heilman *et al.*, 1996). The simplified approach we used to calculate leaf temperature based on the regression between instantaneous PPFD and the temperature difference is only valid for plants under non-limiting water conditions. Very few attempts have been made to perform a calculation of leaf temperature for 3D plants (Dauzat *et al.*, 2001). Recently, a complete coupled model calculating leaf temperature, water status, hydraulic conductance and gas exchange have been developed for grapevine leaves (Zhu *et al.*, 2017). Furthermore, a whole energy balance submodel, considering soil and plant water status have also been introduced in a new model that makes it possible to calculate gas exchange of whole plants under water deficit conditions (Albasha *et al.*, 2019). These studies open the way to evaluating at the whole-canopy level the possibilities of adapting vineyard management to environmental constraints such as water deficit or high temperature that are usually observed in many viticultural regions worldwide. The model developed here represents a robust and promising tool to study and define the optimal plant architecture in order to maximize C allocation or water use efficiency for grapevine plants in the field.

Conclusions

Plant 3D representations have been used to model gas exchange, although very few have been validated at the branch or plant scale. The model developed here was validated with measurements in field-grown plants with four different training systems and over a wide range of environmental conditions. The model showed a low RMSE (2.8 for NCE and 0.55 for Tr) and high agreement index (0.95 for NCE and 0.97 for Tr) for the different training systems evaluated. Accounting for leaf N content distribution within the canopy made it possible to accurately reproduce gas exchange compared with uniform N distributions. One of the major contributions of the model developed here is the coupled simulation of whole-plant photosynthesis and transpiration, opening the way for the comparison of different training systems as regards their water use efficiency.

SUPPLEMENTARY DATA

Supplementary data are available online at https://academic.oup.com/aob and consist of the following.

Figure S1: whole-plant gas exchange chamber design.

Figure S2: effect of plastic film on light intensity and quality.

Figure S3: regression between chamber airflow and pressure transducer.

Figure S4: chamber effect on air temperature and VPD.

Figure S5: comparison between measured and simulated daily integrated light interception efficiency in four trellis systems.

Figure S6: course of instantaneous transpiration rate measured using whole-plant gas exchange chambers and stem heat-balance sap flow.

FUNDING

ACKOWLEDGEMENTS

LITERATURE CITED

Albasha R, Fournier C, Pradal C, *et al.* 2019. HydroShoot: a functional-structural plant model for simulating hydraulic structure, gas and energy exchange dynamics of complex plant canopies under water deficit – application to grapevine (*Vitis vinifera* L.). *In Silico Plants*, in press. doi:10.1093/insilicoplants/diz007.

Braun P, Schmid J. 1999. Sap flow measurements in grapevine (*Vitis vinifera* L.). 1. Stem morphology and use of the heat balance method. *Plant and Soil* **215**: 39–45.

Carbonneau A, Cargnello G. 2003. *Architectures de la vigne et systèmes de conduite.* Paris: Dunod.

Chang TG, Zhao H, Wang N, *et al.* 2019. A three-dimensional canopy photosynthesis model in rice with a complete description of the canopy architecture, leaf physiology, and mechanical properties. *Journal of Experimental Botany* **70**: 2479–2490.

Chelle M, Andrieu B. 1998. The nested radiosity model for the distribution of light within plant canopies. *Ecological Modelling* **111**: 75–91.

Daudet FA, Silvestre J, Ferreira MI, Valancogne C, Pradelle F. 1998. Leaf boundary layer conductance in a vineyard in Portugal. *Agricultural and Forest Meteorology* **89**: 255–267.

Dauzat J, Eroy MN. 1997. Simulating light regime and intercrop yields in coconut based farming systems. *European Journal of Agronomy* **7**: 63–74.

Dauzat J, Rapidel B, Berger A. 2001. Simulation of leaf transpiration and sap-flow in virtual plants: model description and application to a coffee plantation in Costa Rica. *Agricultural and Forest Meteorology* **109**: 143–160.

Dragoni D, Lakso AN, Piccioni RM, Tarara JM. 2006. Transpiration of grapevines in the humid Northeastern United States. *American Journal of Enology and Viticulture* **57**: 460–467.

Escalona JM, Flexas J, Bota J, Medrano H. 2003. Distribution of leaf photosynthesis and transpiration within grapevine canopies under different drought conditions. *Vitis* **42**: 57–64.

Farquhar GD, von Caemmerer S, Berry JA. 1980. A biochemical model of photosynthetic CO_2 assimilation in leaves of C_3 species. *Planta* **149**: 78–90.

Field C. 1983. Allocating leaf nitrogen for the maximization of carbon gain: leaf age as a control on the allocation program. *Oecologia* **56**: 341–347.

Garcia RL, Norman JM, McDermitt DK. 1990. Measurements of canopy gas exchange using an open chamber system. *Remote Sensing Reviews* **5**: 141–162.

Garcia RL, Idso SB, Wall GW, Kimball BA. 1994. Changes in net photosynthesis and growth of *Pinus eldarica* seedlings in response to atmospheric CO_2 enrichment. *Plant, Cell & Environment* **17**: 971–987.

Heilman JL, McInes KJ, Gesch RW, Lascano RJ, Savage MJ. 1996. Effects of trellising on the energy balance of a vineyard. *Agricultural and Forest Meteorology* **81**: 79–93.

Hirose T, Werger MJA. 1987. Maximizing daily canopy photosynthesis with respect to the leaf nitrogen allocation pattern in the canopy. *Oecologia* **72**: 520–526.

Iandolino AB, Pearcy RW, Williams LE. 2013. Simulating three-dimensional grapevine canopies and modelling their light interception characteristics. *Australian Journal of Grape & Wine Research* **19**: 388–400.

Intrieri C, Poni S, Rebucci B, Magnanini E. 1997. Effects of canopy manipulations on whole-vine photosynthesis: results from pot and field experiments. *Vitis* **36**: 167–173.

Intrigliolo DS, Lakso AN. 2011. Effects of light interception and canopy orientation on grapevine water status and canopy gas exchange. *Acta Horticulturae* **889**: 99–104.

Kriedemann PE. 1968. Photosynthesis in vine leaves as a function of light intensity, temperature, and leaf age. *Vitis* **7**: 213–220.

Kull O, Jarvis PG. 1995. The role of nitrogen in a simple scheme to scale up photosynthesis from leaf to canopy. *Plant, Cell & Environment* **18**: 1174–1182.

Kull O, Kruijt B. 1998. Leaf photosynthetic light response: a mechanistic model for scaling photosynthesis to leaves and canopies. *Functional Ecology* **12**: 767–777.

Kull O, Kruijt B. 1999. Acclimation of photosynthesis to light: a mechanistic approach. *Functional Ecology* **13**: 24–36.

Leuning R. 1995. A critical appraisal of a combined stomatal-photosynthesis model for C_3 plants. *Plant, Cell & Environment* **18**: 339–355.

Leuning R, Kelliher FM, de Pury DGG, Schulze ED. 1995. Leaf nitrogen, photosynthesis, conductance and transpiration: scaling from leaves to canopies. *Plant, Cell & Environment* **18**: 1183–1120.

Long SP, Farage PK, Garcia RL. 1996. Measurement of leaf and canopy photosynthetic CO_2 exchange in the field. *Journal of Experimental Botany* **47**: 1629–1642.

Louarn G, Dauzat J, Lecour J, Lebon E. 2008*a*. Influence of trellis system and shoot positioning on light interception and distribution in two grapevine cultivars with different architectures: an original approach based on 3D canopy modelling. *Australian Journal of Grape & Wine Research* **14**: 143–152.

Louarn G, Lecoeur J, Lebon E. 2008*b*. A three dimensional statistical reconstruction model of grapevine (*Vitis vinifera* L.) simulating canopy structure variability within and between cultivar/training system pairs. *Annals of Botany* **101**: 1167–1184.

Louarn G, Frak E, Zaka S, Prieto JA, Lebon E. 2015. An empirical model that uses light attenuation and plant nitrogen status to predict within-canopy N distribution and upscale photosynthesis from leaf to whole canopy. *AoB Plants,* doi:10.1093/aobpla/plv116.

Mabrouk H, Sinoquet H. 1998. Indices of light microclimate and canopy structure of grapevines determined by 32D digitizing and image analysis, and their relationship to grape quality. *Australian Journal of Grape & Wine Research* **4**: 2–13.

Mabrouk H, Carbonneau A, Sinoquet H. 1997. Canopy structure and radiation regime in grapevine. I. Spatial and angular distribution of leaf area in two canopy systems. *Vitis* **36**: 119–123.

Massonnet C, Regnard JL, Lauri PE, Costes E, Sinoquet H. 2008. Contributions of foliage distribution and leaf functions to light interception, transpiration and photosynthetic capacities in two apple cultivars at branch and tree scales. *Tree Physiology* **28**: 665–678.

Medrano H, Tomas M, Martorell S, *et al.* 2015. Improving water used efficiency of vineyards in semi-arid regions. A review. *Agronomy for Sustainable Development* **35**: 499–517.

Merli MC, Gatti M, Galbignani M, Bernizzoni F, Magnanini E, Poni S. 2015. Water use efficiency in Sangiovese grapes (*Vitis vinifera* L.) subjected to water stress before veraison: different levels of assessment lead to different conditions. *Functional Plant Biology* **42**: 198–208.

Müller J, Braune H, Diepenbrock W. 2008. Photosynthesis-stomatal conductance model LEAFC3-N: specification for barley, generalised nitrogen relations, and aspects of model application. *Functional Plant Biology* **35**: 797–810.

Niinemets Ü, Tenhunen JD. 1997. A model separating leaf structural and physiological effects on carbon gain along light gradients for the shade-tolerant species *Acer saccharum*. *Plant, Cell & Environment* **20**: 845–866.

Niinemets Ü, Anten N. 2009. Packing the photosynthetic machinery: from leaf to canopy. In: Nedbal L, Govindjee AL, eds. *Photosynthesis in silico: understanding complexity from molecules to ecosystems*. Netherlands: Springer Science + Business Media, 363–399.

Perez Peña J, Tarara J. 2004. A whole canopy gas exchange system for several mature field-grown grapevines. *Vitis* **43**: 7–14

Poirier-Pocovi M, Lothier J, Buck-Sorlin G. 2018. Modelling temporal variation of parameters used in two photosynthesis models: influence of fruit load and girdling on leaf photosynthesis in fruit-bearing branches of apple. *Annals of Botany* **121**: 821–832.

Poni S, Merli MC, Magnanini E, *et al.* 2014*a*. An improved multichamber gas exchange system for determining whole-canopy water-use efficiency in grapevine. *American Journal of Enology and Viticulture* **5**: 268–276.

Poni S, Galbignani M, Magnani E, *et al.* 2014*b*. The isohydric cv. Montepulciano (*Vitis vinifera* L.) does not improve its whole-plant water use efficiency when subjected to pre-veraison water stress. *Scientia Horticulturae* **179**: 103–111.

Pradal C, Dufour-Kowalski S, Boudon F, Fournier C, Godin C. 2008. OpenAlea: a visual programming and component-based software platform for plant modelling. *Functional Plant Biology* **35**: 751–760.

Prieto JA, Louarn G, Perez Pena J, Ojeda H, Simonneau T, Lebon E. 2012. A leaf gas exchange model that accounts for intra-canopy variability by considering leaf nitrogen content and local acclimation to radiation in grapevine (*Vitis vinifera* L.). *Plant, Cell & Environment* **35**: 1313–1328.

de Pury DGG, Farquhar GD. 1997. Simple scaling of photosynthesis from leaves to canopies without the errors of big-leaf models. *Plant, Cell & Environment* **20**: 537–557.

Rakocevic M, Ribeiro RV, Ribeiro Marchiori PE, Filizola HF, Batista ER. 2018. Structural and functional changes in coffee trees after 4 years under free air CO2 enrichment. *Annals of Botany* **121**: 1065–1078.

Reynolds AG, Vandel Heuvel JE. 2009. Influence of grapevine training systems on vine growth and fruit composition: a review. *American Journal of Enology and Viticulture* **60**: 251–268.

Ripullone F, Grassi G, Lauteri M, Borghetti M. 2003. Photosynthesis-nitrogen relationships: interpretation of different patterns between *Pseudotsuga menziesii* and *Populus × euroamericana* in a mini-stand experiment. *Tree Physiology* **23**: 137–144.

Le Roux X, Grand S, Dreyer E, Daudet FA. 1999. Parameterization and testing of a biochemically based photosynthesis model for walnut (*Juglans regia*) trees and seedlings. *Tree Physiology* **19**: 481–492.

Sarlikioti V, de Visser PHB, Marcelis LFM. 2011. Exploring the spatial distribution of light interception and photosynthesis of canopies by means of a functional-structural plant model. *Annals of Botany* **107**: 875–883.

Schultz HR. 1995. Grape canopy structure, light microclimate and photosynthesis. I. A two-dimensional model of the spatial distribution of surface area densities and leaf ages in two canopy systems. *Vitis* **34**: 211–215.

Sinoquet H, Thanisawanyangkura S, Mabrouk H, Kasemsap P. 1998. Characterization of the light environment in canopies using 3D digitising and image processing. *Annals of Botany* **82**: 203–212.

Sinoquet H, Le Roux X, Adam B, Ameglio T, Daudet FA. 2001. RATP: a model for simulating the spatial distribution of radiation absorption, transpiration and photosynthesis within canopies: application to an isolated tree crown. *Plant, Cell & Environment* **24**: 395–406.

Smart RE. 1985. Principles of grapevine canopy microclimate manipulation with implications for yield and quality: a review. *American Journal of Enology and Viticulture* **35**: 230–239.

Smart RE, Dick JK, Gravett IM, Fisher BM. 1990. Canopy management to improve grape yield and wine quality: principles and practices. *South African Journal of Enology and Viticulture* **11**: 1–17.

Tarara JM, Perez Peña J. 2015. Moderate water stress from regulated deficit irrigation decreases transpiration similarly to net carbon exchange in grapevine canopies. *Journal of the American Society for Horticultural Science* **140**: 413–426.

Tarara JM, Perez Peña J, Keller M, Schreiner RP, Smithyman RP. 2011. Net carbon exchange in grapevine canopies responds rapidly to timing and extent of regulated deficit irrigation. *Functional Plant Biology* **38**: 386–400.

Valancogne C, Granier A. 1991. Intérêt des méthodes thermiques de mesure de flux de sève pour l'étude du bilan hydrique des savanes. In: *Soil Water Balance in the Sudano-Sahelian Zone (Proceedings of the Niamey Workshop, February 1991)*. IAHS *Publication No. 199*, Wallingford, UK: International Association of Hydrological Sciences, 387–400.

Vos J, Evers JB, Buck-Sorlin GH, Andrieu B, Chelle M, de Visser PHB. 2010. Functional-structural plant modeling: a new versatile tool in crop science. *Journal of Experimental Botany* **61**: 2101–2115.

Wang M, White N, Grimm V, *et al.* 2018. Pattern-oriented modelling as a novel way to verify and validate functional–structural plant models: a demonstration with the annual growth module of avocado. *Annals of Botany* **121**: 941–959.

Williams LE, Ayars JE. 2005. Grapevine water use and the crop coefficient are linear functions of the shaded area beneath the canopy. *Agricultural and Forest Meteorology* **132**: 201–211.

Willmott CJ. 1982. Some comments on the evaluation of model performance. *Bulletin American Meteorological Society* **63**: 1309–1313.

Zhu J, Dai Z, Vivin P, *et al.* 2017. A 3-D functional–structural grapevine model that couples the dynamics of water transport with leaf gas exchange. *Annals of Botany* **121**: 833–848.